Cent. Eur. J. Geosci. • 6(3) • 2014 • 373-392
DOI: 10.2478/s13533-012-0183-y

VERSITA

Central European Journal of **Geosciences**

A case study for the integration of predictive mineral potential maps

Research Article

Saro Lee[1], Hyun-Joo Oh[2]*, Chul-Ho Heo[2], Inhye Park[1]

1 Geological Mapping Department, Korea Institute of Geoscience Mineral Resources (KIGAM), 124 Gwahang-no, Yuseong-gu, Daejeon 305-350, South Korea

2 Mineral Resources Research Department, Korea Institute of Geoscience Mineral Resources (KIGAM), 124 Gwahang-no, Yuseong-gu, Daejeon 305-350, South Korea

Received 9 December 2013; accepted 22 May 2014

Abstract: This study aims to elaborate on the mineral potential maps using various models and verify the accuracy for the epithermal gold (Au) – silver (Ag) deposits in a Geographic Information System (GIS) environment assuming that all deposits shared a common genesis. The maps of potential Au and Ag deposits were produced by geological data in Taebaeksan mineralized area, Korea. The methodological framework consists of three main steps: 1) identification of spatial relationships 2) quantification of such relationships and 3) combination of multiple quantified relationships. A spatial database containing 46 Au-Ag deposits was constructed using GIS. The spatial association between training deposits and 26 related factors were identified and quantified by probabilistic and statistical modelling. The mineral potential maps were generated by integrating all factors using the overlay method and recombined afterwards using the likelihood ratio model. They were verified by comparison with test mineral deposit locations. The verification revealed that the combined mineral potential map had the greatest accuracy (83.97%), whereas it was 72.24%, 65.85%, 72.23% and 71.02% for the likelihood ratio, weight of evidence, logistic regression and artificial neural network models, respectively. The mineral potential map can provide useful information for the mineral resource development.

Keywords: GIS • likelihood ratio • weight of evidence • logistic regression • artificial neural network • mineral potential mapping

1. Introduction

Many probabilistic, statistical and data mining models have been proposed for mineral potential mapping. They include logistic regression [6, 7, 13, 15, 37], frequency ratio [27, 29, 38], weights of evidence [3, 8, 35, 39], Dempster-Shafer [27, 34], support vector machine [36, 44], Bayesian network classifiers [32], fuzzy logic [14, 20, 33], and artificial neural networks [4, 28, 31, 40–42, 45]. All of these approaches have been applied to mineral resource appraisal and others. But the studies have applied model separately. There are no studies which combine the results of mineral potential. So, the difference of the study is to combine the results of mineral potential, which have made from 4 different models to make better accurate mineral potential map.

This application builds a model using observations about the association of mineral occurrences with various geological features in a quantitative manner. For the applica-

*E-mail: ohj@kigam.re.kr

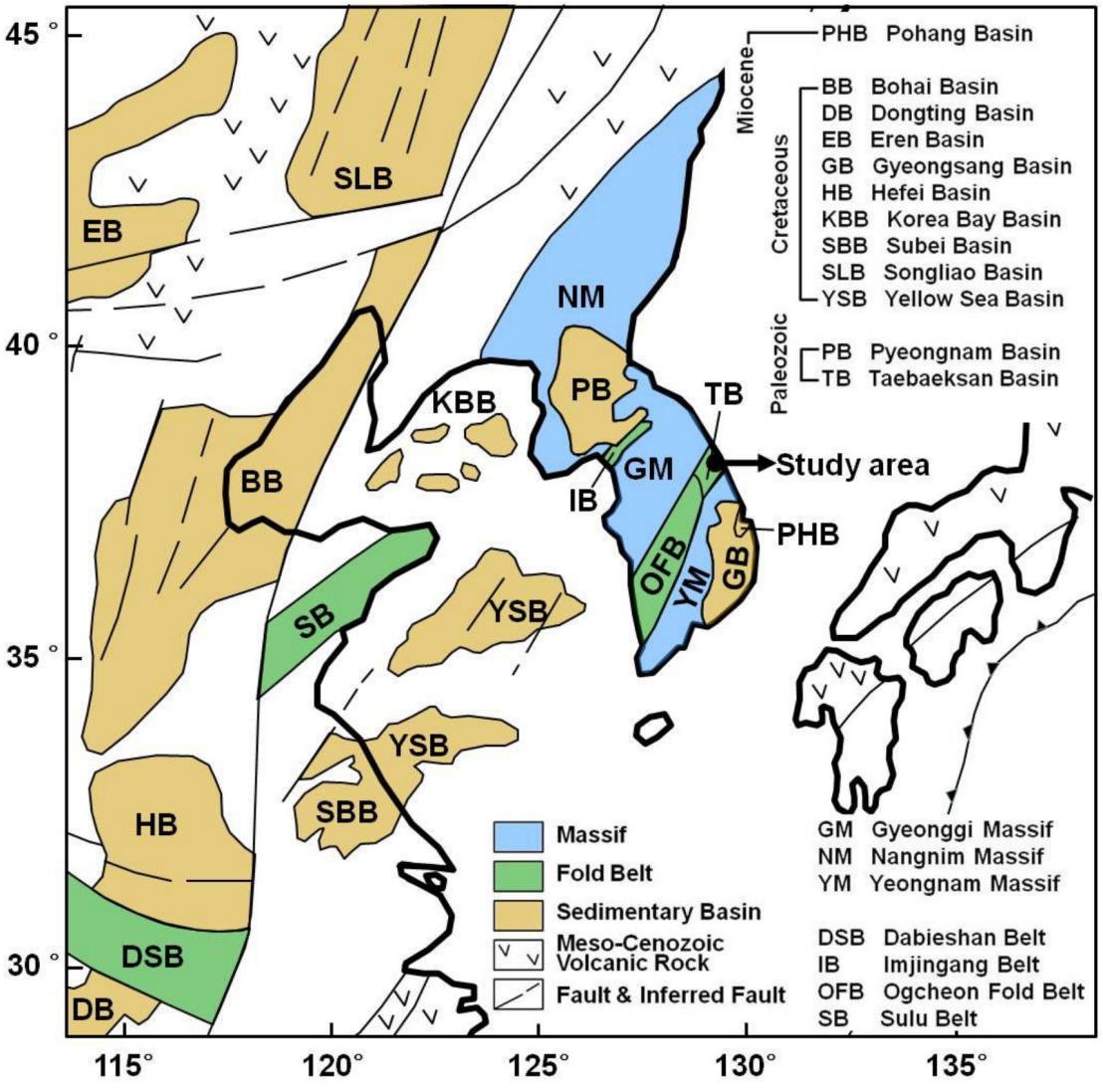

Figure 1. Study area with tectonic boundary in the northeast Asian margin modified from Chough et al. 2000 [12].

tion, GIS was used to combine and analyze a variety of geoscientific data, including geological, geochemical and geophysical maps. The GIS is the best tool for analyzing all kinds of geospatial data in mineral exploration and delivering the means to organize the mineral exploration process. The objective of this study is to combine Au-Ag potential maps using likelihood ratio, weight of evidence, logistic regression and artificial neural network models and verify and compare the combined mineral potential map with each mineral potential map in the Taebaeksan mineralized area of Korea (Figure 1). This region has many mineral deposits and geological, geochemical and geophysical survey data available and high mineral potential, which is referred to Oh and Lee [29]. The preparation of mineral potential maps using GIS (ArcGIS 10) was accomplished in five major steps (Figure 2). (1) Compilation of a spatial database. A total of 46 Au-Ag mineral deposits were used to create a spatial database using GIS. Geological, geochemical and geophysical maps were similarly treated. (2) Processing the data from the database. Using the GIS overlay method, the mineral deposits and the factors were combined and their relationships were determined quantitatively using likelihood ratio, weight of evidence, logistic regression and artificial neural network models. (3) Application of an each model to generate a mineral potential map. (4) Combination of the mineral potential maps using likelihood ratio. (5) Verification and comparison of each mineral potential map and combined mineral potential map using test mineral deposits that were not used directly in the analysis.

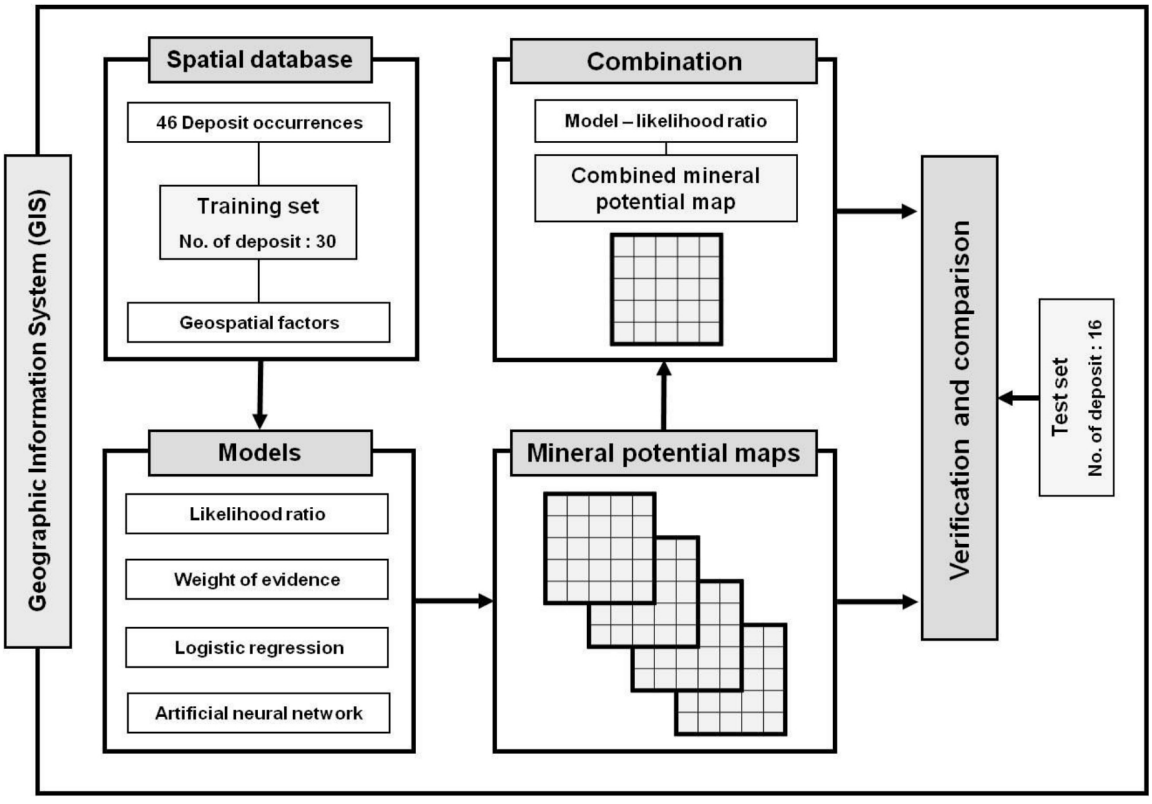

Figure 2. Study flow.

The data-processing step involves numerous operations to extract and enhance predictive criteria from each of the initial data layers. Combination modeling refers to the methods used for combining predictive-data layers into a mineral potential map. The map does not estimate the number and size of mineral deposits, but indicates, on a broad scale, areas considered to be prospective for exploration.

2. Geological setting of the Taebaeksan basin

The Taebaeksan basin (TB) lies in the central east part of the Korean Peninsula and includes the Taebaeksan mineralized area, located within latitudes 37°15′24′′–37°30′00′′ N and longitudes 128°30′30′′–129°02′40′′ E (Figure 1). The study area occupies approximately 1,050 km^2.

The Korean peninsula is located on the northeastern margin of the Eurasian plate. The major tectonostratigraphic units of South Korea include the Gyeonggi Massif (GM), the Ogcheon Fold Belt (OFB), the Yeongnam Massif (YM), and the Gyeongsang Basin (GB) (Figure 1). The TB occupies the northeastern part of the Korean peninsula and is composed primarily of the Cambrian–Ordovician-aged Joseon Supergroup and Carboniferous–Triassic-aged Pyeongan Supergroup. The Joseon Supergroup rests unconformably on the Precambrian-aged granitic gneiss and metasedimentary rocks of the YM and is overlain unconformably by the Pyeongan Supergroup [9]. The lower Paleozoic sediments are primarily shallow marine in origin and consist predominantly of carbonates with lesser amounts of sandstone and shale, whereas the Pyeongan Supergroup is comprised of thick clastic successions of marginal marine to nonmarine environments containing economically important coal measures [10, 12]. The Late Carboniferous to Triassic sedimentary rocks of the Pyeongan Supergroup are well exposed in the TB. These deposits consist predominantly of shale and sandstone with small amounts of limestone, conglomerate and coal. Throughout much of the TB, they rest unconformably on the Joseon Supergroup, except in the Jeongseon area. The Pyeongan sedimentation initiated in a marginal marine environment in the Late Carboniferous with a brief interruption in deposition, presumably in the latest Carboniferous to earliest Permian, followed by the deposition of a thick non-marine sandstone–shale succession in the Permian [10, 12].

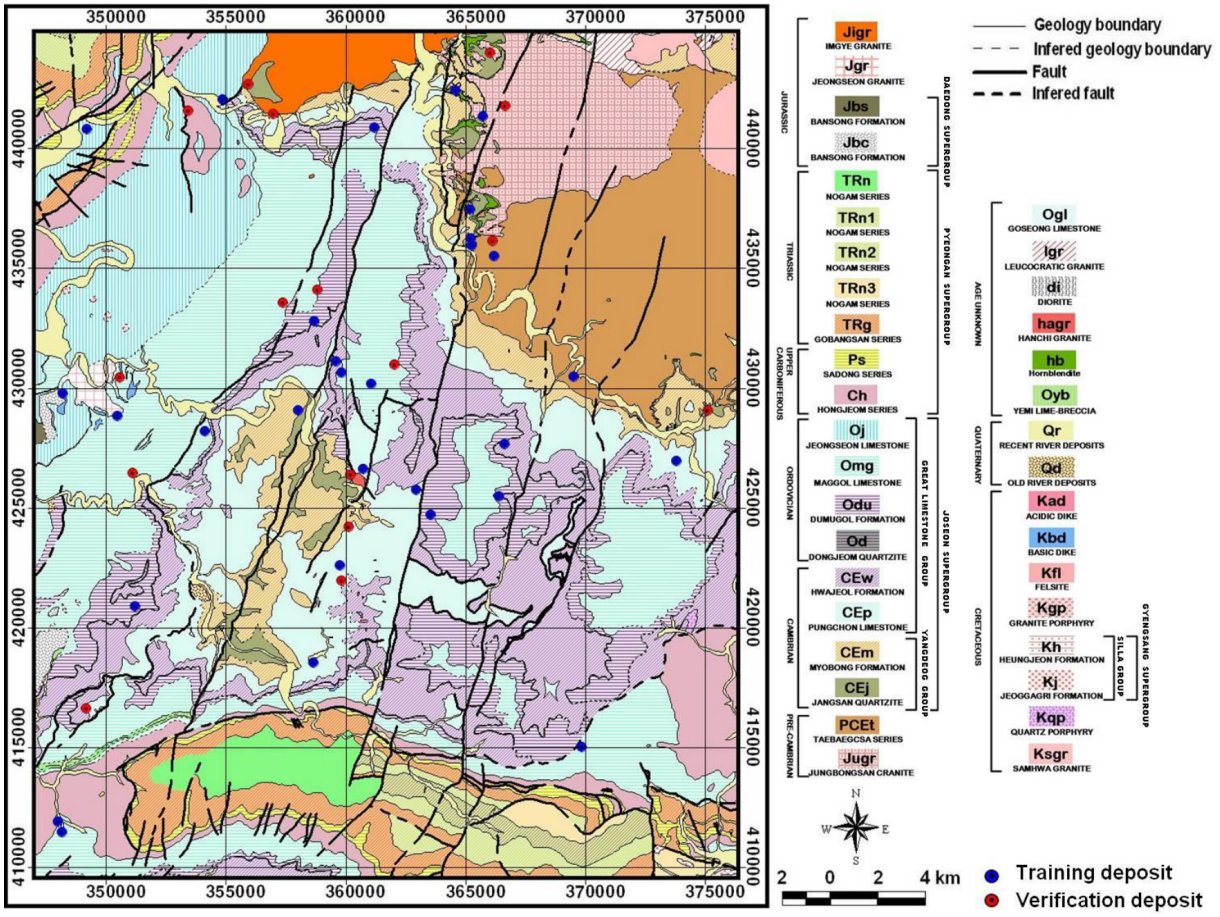

Figure 3. Geological map with mineral deposits (Combined geological map of Jeongseon, Imgye, Yemi and Homyeong sheets produced by the Korea Institute of Geoscience & Mineral Resources at 1:50,000).

3. Mineralization of study area

The Taebaeksan mineralized area is the most important deposit in South Korea and is located in TB. The study area has a long history of metal production from veins and skarns in sediments near granitoid intrusions [30]. The mineralized area is rich in Pb-Zn-W-Fe-Cu-Mo-Au-Ag mineral resources with a diversity of deposit styles. These deposits principally coexist in time and space with porphyry-related epigenetic deposit types such as skarns, hydrothermal replacement, mesothermal veins, and Carline-like deposits. In the study area, the gold-silver deposits are of an epithermal type related to granites. The main opaque minerals include electrum, pyrite, arsenopyrite, stibnite, and sphalerite. Some polished and microprobe sections of samples from structures cutting through Cambrian oolitic limestone show zones of gold and arsenic enrichment along the perimeters of pyrite grains [30]. The occurrence of gold deposits that are stratigraphically localized in crystalline limestone and altered argillaceous sediments is indicative of disseminated gold. The arsenic anomaly has been shown to be related to metalliferous ore deposits (mainly Ag-Au), which are closely associated with the Sb anomaly. Some elements in the altered limestones in the study such as Au, Ag, As, Sb, Cu, Pb, Zn, and Mo are closely associated together [43].

The bedrock consists of Precambrian metamorphic and metasedimentary rocks (the units Jugr and PCEt as shown in Figure 3), Paleozoic and Mesozoic sedimentary rocks (the units CEj, CEm, CEp, CEw, Od, Odu, Omg, Oj, Ch, Ps, TRg, TRn, TRn1, TRn2, TRn3, Jbc and Jbs), Mesozoic volcanic rocks (the unit Jgr) and plutons (the unit Jigr), and minor occurrences of Quaternary sediments (the units Qd and Qr) [16]. Geologic structures in the eastern part of the TB suggest that the sequence underwent four deformational stages [18, 19]. A D1 deformation event of unknown age generated NE-striking ductile shear zones with a reverse sense of slip between the Precambrian massif and early Paleozoic sequences [17–19]. During the D2 deformation

(the Songrim orogeny), NE-trending folds and thrusts were generated with mostly SE vergence. D3 deformation (the Daebo event) then produced NE-trending folds and thrusts with a SE vergence. During the late Cretaceous to early Tertiary Bulgugsa event, the entire sequence underwent D4 deformation that caused E–W trending folds and faults [18]. Gold and silver bearing hydrothermal vein deposits in the study area occur in various host lithologies, consist of multiple generations of quartz and/or carbonates with base metal sulfides, and have NNW, NS or NNE strikes, which seem to be related to NE strike-slip faults [21, 23].

4. Spatial database

Data on 46 epithermal Au-Ag deposits were selected in mineral deposit maps of the Taebaeksan mineralization with mineral variety and type, which were obtained from the MIRECO (Mine Reclamation Crop.), NHMRG (Natural Hazard Mitigation Research Group) and KIGAM (Korea Institute of Geoscience and Mineral Resources). The 26 factors related to Au-Ag mineral occurrence are the geological data of lithology and fault structure, geochemical data including the presence of Al, As, Ba, Ca, Cd, Co, Cr, Cu, Fe, K, Li, Mg, Mn, Na, Ni, Pb, Si, Sr, V, W, Zn, Cl^- and F^-, and the geophysical data on the magnetic anomalies [11, 24]. All of these factors were compiled in the GIS database.

The geological data were derived from a 1:50,000 geological map (Figure 3). The lithology and distance from fracture were registered. The geochemical data were acquired through a stream water and sediment geochemical survey. The geochemical maps were made from interpolation of values of geochemical elements. The geophysical data were acquired through airborne magnetic [22]. Then the data were interpolated to make the geophysical map. All factors were converted to raster form. In this study we use 30 m × 30 m considering input data map scale (1:50,000). The numbers of rows and columns are 986 and 1,183, and the total number of cells in the study area is 1,166,438. Total number of Au-Ag mineral deposits is 46 including 30 training and 16 verification deposits, which were randomly selected.

In GIS, when converting vector to raster, if there are more than two attributes, the attribute which occupies the largest area is selected as the representative cell. The remaining attributes are ignored. Therefore, the selection of cell size is important. Because the cell size is too big, many attributes can be ignored and the cell size is too small, the file size is too big and computing time is too long. So, based on the input data scale, the adequate cell size was selected for the minimum loss of data and computing efficiency. Usually, in the 1:250,000 scale the 100 m cell size is used and in the 1:50,000 scale the 30 m cell size is used.

5. Model

5.1. Likelihood ratio

The strength of the spatial relationship between deposit occurrence and its related factor is expressed in terms of the likelihood ratio in the study. Likelihood ratio is the ratio of probability of a deposit occurrence (D) to its non-occurrence for the class i of factor B. The likelihood ratios [2], which are sufficiency ratio (LS) and necessity ratio (LN), are required by the following Equations (1) and (2):

$$LS_i = \frac{P(B_i|D)}{P(B_i|\bar{D})} \tag{1}$$

$$LN_i = \frac{P(\bar{B}_i|D)}{P(\bar{B}_i|\bar{D})} \tag{2}$$

So, the ratio is higher than 1, the higher relationship between deposit occurrence and the certain factors' class and the ratio is lower than 1, the lower relationship between deposit occurrence and the certain factors' class. The likelihood ratio value was set to the range of each factor values, which are reclassified into 10 classes by equal area. The likelihood ratios for each factors' range or class (Table 1) were summed to calculate MPIL (Mineral Potential Index), as shown in Equation (3) and Figure 4:

$$MPI_L = \sum LS \tag{3}$$

where LS = likelihood ratio (e.g., sufficiency ratio) for each factors' range or class.

5.2. Weight of evidence

Weight of evidence modelling formulated for mineral potential assessment was first described by Bonham-Carter and others [3]. The weights of evidence analysis result in a set of statistically derived values reflecting the spatial association between deposit occurrence and a binary pattern of a factor. To generate the binary patterns for the occurrence-related factors, they were classified into binary maps as calculating W^+ and W^- from Equations (4) and (5), and showing favorable and unfavorable areas.

$$W_i^+ = \log_e LS_i \tag{4}$$

$$W_i^- = \log_e LN_i \tag{5}$$

Table 1. Spatial relationship between mineral deposits and its related factors.

Factor	Likelihood ratio						Weight of evidence				Logistic	ANN
	Class[a]	No. of pixels	%Area	Mineral occ.	%occ.	LS	W^+	W^-	C	C/S(c)	Coefficient	Weight
Al (ppb)	26.00-44.15	116666	10.00	3	10.00	1.00	0.00	0.00	0.00	0	0.01065	0.032
	44.16-84.54	116651	10.00	2	6.67	0.67	-0.41	0.04	-0.44	-0.6		
	84.55-103.39	116737	10.01	4	13.33	1.33	0.29	-0.04	0.32	0.6		
	103.40-112.87	116716	10.01	2	6.67	0.67	-0.41	0.04	-0.44	-0.6		
	112.88-119.29	116695	10.00	7	23.33	2.33	0.85	-0.16	1.01	2.33		
	119.30-124.97	116601	10.00	7	23.33	2.33	0.85	-0.16	1.01	2.34		
	124.98-133.04	116613	10.00	1	3.33	0.33	-1.10	0.07	-1.17	-1.15		
	133.05-164.69	116594	10.00	2	6.67	0.67	-0.41	0.04	-0.44	-0.6		
	164.70-231.11	116586	10.00	2	6.67	0.67	-0.40	0.04	-0.44	-0.6		
	231.12-499.99	116579	9.99	0	0.00	0.00	NaN	0.11	NaN	NaN		
As (ppm)	1.01-14.58	116689	10.00	0	0.00	0.00	NaN	0.11	NaN	NaN	0.02370	0.034
	14.59-21.78	116779	10.01	7	23.33	2.33	0.85	-0.16	1.01	2.33		
	21.79-27.56	116734	10.01	0	0.00	0.00	NaN	0.11	NaN	NaN		
	27.57-35.09	116702	10.00	2	6.67	0.67	-0.41	0.04	-0.44	-0.6		
	35.10-43.43	116782	10.01	1	3.33	0.33	-1.10	0.07	-1.17	-1.15		
	43.44-47.59	116901	10.02	4	13.33	1.33	0.29	-0.04	0.32	0.6		
	47.60-49.47	116516	9.99	0	0.00	0.00	NaN	0.11	NaN	NaN		
	49.48-49.99	65606	5.62	3	10.00	1.78	0.58	-0.05	0.62	1.02		
	50.00	283729	24.32	13	43.33	1.78	0.58	-0.29	0.87	2.35		
Ba (ppb)	2.00-3.99	117477	10.07	0	0.00	0.00	NaN	0.11	NaN	NaN	0.05914	0.041
	4.00-5.96	116734	10.01	7	23.33	2.33	0.85	-0.16	1.01	2.33		
	5.97-7.04	117258	10.05	2	6.67	0.66	-0.41	0.04	-0.45	-0.61		
	7.05-7.86	116532	9.99	3	10.00	1.00	0.00	0.00	0.00	0		
	7.87-8.55	116787	10.01	5	16.67	1.66	0.51	-0.08	0.59	1.2		
	8.56-9.61	116822	10.02	4	13.33	1.33	0.29	-0.04	0.32	0.6		
	9.62 -10.87	116583	9.99	2	6.67	0.67	-0.40	0.04	-0.44	-0.6		
	10.88-13.28	116120	9.96	1	3.33	0.33	-1.09	0.07	-1.17	-1.15		
	13.29-17.38	116242	9.97	3	10.00	1.00	0.00	0.00	0.00	0.01		
	17.39-200.97	115883	9.93	3	10.00	1.01	0.01	0.00	0.01	0.01		
Ca (ppm)	1.53-6.24	116712	10.01	2	6.67	0.67	-0.41	0.04	-0.44	-0.6	-0.00002	0.036
	6.25-18.99	116637	10.00	4	13.33	1.33	0.29	-0.04	0.33	0.61		
	19.00-28.24	116714	10.01	1	3.33	0.33	-1.10	0.07	-1.17	-1.15		
	28.25-35.41	116742	10.01	3	10.00	1.00	0.00	0.00	0.00	0		
	35.42-40.44	116662	10.00	2	6.67	0.67	-0.41	0.04	-0.44	-0.6		
	40.45-43.42	116679	10.00	2	6.67	0.67	-0.41	0.04	-0.44	-0.6		
	43.43-46.01	116621	10.00	2	6.67	0.67	-0.41	0.04	-0.44	-0.6		
	46.02-48.04	117223	10.05	4	13.33	1.33	0.28	-0.04	0.32	0.6		
	48.05-49.16	116647	10.00	5	16.67	1.67	0.51	-0.08	0.59	1.2		
	49.17-50.00	115801	9.93	5	16.67	1.68	0.52	-0.08	0.60	1.22		
Cd (ppm)	1.0000-1.1008	116740	10.01	3	10.00	1.00	0.00	0.00	0.00	0	-0.20344	0.035
	1.1009-1.2239	116647	10.00	3	10.00	1.00	0.00	0.00	0.00	0		
	1.2240-1.3473	116690	10.00	2	6.67	0.67	-0.41	0.04	-0.44	-0.6		
	1.3474-1.4928	116699	10.00	2	6.67	0.67	-0.41	0.04	-0.44	-0.6		
	1.4929-1.6538	116626	10.00	5	16.67	1.67	0.51	-0.08	0.59	1.2		
	1.6539-1.8480	116640	10.00	4	13.33	1.33	0.29	-0.04	0.33	0.61		
	1.8481-1.9829	116621	10.00	2	6.67	0.67	-0.41	0.04	-0.44	-0.6		
	1.9830-2.2506	116610	10.00	5	16.67	1.67	0.51	-0.08	0.59	1.2		
	2.2507-3.2164	116585	9.99	1	3.33	0.33	-1.10	0.07	-1.17	-1.15		
	3.2165-9.9992	116580	9.99	3	10.00	1.00	0.00	0.00	0.00	0		

Factor	Likelihood ratio						Weight of evidence				Logistic	ANN
	Class[a]	No. of pixels	%Area	Mineral occ.	%occ.	LS	W^+	W^-	C	C/S(c)	Coefficient	Weight
Cl^- (ppm)	1.0106-2.2074	116644	10.00	1	3.33	0.33	-1.10	0.07	-1.17	-1.15	0.00004	0.041
	2.2075-2.4546	116681	10.00	0	0.00	0.00	NaN	0.11	NaN	NaN		
	2.4547-2.7386	116654	10.00	3	10.00	1.00	0.00	0.00	0.00	0		
	2.7387-2.9874	116642	10.00	4	13.33	1.33	0.29	-0.04	0.33	0.61		
	2.9875-3.2353	116647	10.00	0	0.00	0.00	NaN	0.11	NaN	NaN		
	3.2354-3.4804	116642	10.00	7	23.33	2.33	0.85	-0.16	1.01	2.33		
	3.4805-3.8803	116637	10.00	5	16.67	1.67	0.51	-0.08	0.59	1.2		
	3.8804-4.7479	116635	10.00	5	16.67	1.67	0.51	-0.08	0.59	1.2		
	4.7480-5.9843	116628	10.00	2	6.67	0.67	-0.41	0.04	-0.44	-0.6		
	5.9844-27.6669	116628	10.00	3	10.00	1.00	0.00	0.00	0.00	0		
Co (ppb)	1.0000-1.5665	116648	10.00	4	13.33	1.33	0.29	-0.04	0.33	0.61	-0.78378	0.041
	1.5666-2.5807	116657	10.00	1	3.33	0.33	-1.10	0.07	-1.17	-1.15		
	2.5808-1.9789	116722	10.01	5	16.67	1.67	0.51	-0.08	0.59	1.2		
	1.9790-3.1012	116636	10.00	1	3.33	0.33	-1.10	0.07	-1.17	-1.15		
	3.1013-3.3506	116651	10.00	3	10.00	1.00	0.00	0.00	0.00	0		
	3.3507-3.6660	116656	10.00	2	6.67	0.67	-0.41	0.04	-0.44	-0.6		
	3.6661-3.9952	116621	10.00	4	13.33	1.33	0.29	-0.04	0.33	0.61		
	3.9953-4.4250	116620	10.00	7	23.33	2.33	0.85	-0.16	1.01	2.33		
	4.4251-5.0758	116620	10.00	2	6.67	0.67	-0.41	0.04	-0.44	-0.6		
	5.0759-9.9999	116607	10.00	1	3.33	0.33	-1.10	0.07	-1.17	-1.15		
Cr (ppb)	1.0000-1.1958	116649	10.00	6	20.00	2.00	0.69	-0.12	0.81	1.78	0.03562	0.040
	1.1959-1.3244	116645	10.00	0	0.00	0.00	NaN	0.11	NaN	NaN		
	1.3245-1.4319	116772	10.01	2	6.67	0.67	-0.41	0.04	-0.44	-0.61		
	1.4320-1.5656	116663	10.00	5	16.67	1.67	0.51	-0.08	0.59	1.2		
	1.5657-1.8305	116650	10.00	4	13.33	1.33	0.29	-0.04	0.33	0.61		
	1.8306-2.0343	116653	10.00	3	10.00	1.00	0.00	0.00	0.00	0		
	2.0344-2.3185	116625	10.00	4	13.33	1.33	0.29	-0.04	0.33	0.61		
	2.3186-2.7629	116602	10.00	1	3.33	0.33	-1.10	0.07	-1.17	-1.15		
	2.7630-3.2865	116601	10.00	5	16.67	1.67	0.51	-0.08	0.59	1.2		
	3.2866-9.9987	116578	9.99	0	0.00	0.00	NaN	0.11	NaN	NaN		
Cu (ppb)	1.000-2.034	116889	10.02	1	3.33	0.33	-1.10	0.07	-1.17	-1.15	-0.57369	0.037
	2.035-2.450	116787	10.01	4	13.33	1.33	0.29	-0.04	0.32	0.6		
	2.451-2.744	116603	10.00	4	13.33	1.33	0.29	-0.04	0.33	0.61		
	2.745-2.994	117174	10.05	6	20.00	1.99	0.69	-0.12	0.81	1.77		
	2.995-3.262	116784	10.01	6	20.00	2.00	0.69	-0.12	0.81	1.77		
	3.263-3.669	116566	9.99	2	6.67	0.67	-0.40	0.04	-0.44	-0.6		
	3.670-3.977	116422	9.98	3	10.00	1.00	0.00	0.00	0.00	0		
	3.978-4.710	116412	9.98	2	6.67	0.67	-0.40	0.04	-0.44	-0.6		
	4.711-7.695	116407	9.98	1	3.33	0.33	-1.10	0.07	-1.17	-1.15		
	7.696-2.9999	116394	9.98	1	3.33	0.33	-1.10	0.07	-1.17	-1.15		
F^- (ppm)	0.03-0.14	117101	10.04	5	16.67	1.66	0.51	-0.08	0.58	1.19	-0.00701	0.038
	0.15-0.15	116775	10.01	2	6.67	0.67	-0.41	0.04	-0.44	-0.61		
	0.16-0.16	117073	10.04	3	10.00	1.00	0.00	0.00	0.00	-0.01		
	0.17-0.17	117348	10.06	3	10.00	0.99	-0.01	0.00	-0.01	-0.01		
	0.18-0.18	117148	10.04	2	6.67	0.66	-0.41	0.04	-0.45	-0.61		
	0.19-0.20	116558	9.99	5	16.67	1.67	0.51	-0.08	0.59	1.2		
	0.21-0.22	116117	9.95	4	13.33	1.34	0.29	-0.04	0.33	0.62		
	0.23-0.24	116151	9.96	2	6.67	0.67	-0.40	0.04	-0.44	-0.6		
	0.25-0.28	116321	9.97	3	10.00	1.00	0.00	0.00	0.00	0.01		
	0.29-1.99	115846	9.93	1	3.33	0.34	-1.09	0.07	-1.16	-1.14		

Factor	Likelihood ratio						Weight of evidence				Logistic	ANN
	Class[a]	No. of pixels	%Area	Mineral occ.	%occ.	LS	W^+	W^-	C	C/S(c)	Coefficient	Weight
Fe (ppm)	2.00-6.77	117031	10.03	2	6.67	0.66	-0.41	0.04	-0.45	-0.61	0.00001	0.030
	6.78-7.86	116771	10.01	5	16.67	1.66	0.51	-0.08	0.59	1.2		
	7.87-8.88	116611	10.00	4	13.33	1.33	0.29	-0.04	0.33	0.61		
	8.89-9.91	117384	10.06	4	13.33	1.32	0.28	-0.04	0.32	0.59		
	9.92-11.12	116592	10.00	6	20.00	2.00	0.69	-0.12	0.81	1.78		
	11.13-12.99	116876	10.02	1	3.33	0.33	-1.10	0.07	-1.17	-1.15		
	13.00-15.76	116535	9.99	2	6.67	0.67	-0.40	0.04	-0.44	-0.6		
	15.77-21.24	116233	9.96	2	6.67	0.67	-0.40	0.04	-0.44	-0.6		
	21.25-35.77	116234	9.96	3	10.00	1.00	0.00	0.00	0.00	0.01		
	35.78-99.99	116171	9.96	1	3.33	0.33	-1.09	0.07	-1.17	-1.15		
K (ppm)	0.1201-0.3403	116712	10.01	2	6.67	0.67	-0.41	0.04	-0.44	-0.6	-0.00080	0.037
	0.3404-0.4005	116798	10.01	1	3.33	0.33	-1.10	0.07	-1.17	-1.15		
	0.4006-0.4634	116644	10.00	4	13.33	1.33	0.29	-0.04	0.33	0.61		
	0.4635-0.5461	116707	10.01	2	6.67	0.67	-0.41	0.04	-0.44	-0.6		
	0.5462-0.6365	116600	10.00	5	16.67	1.67	0.51	-0.08	0.59	1.2		
	0.6366-0.7389	116663	10.00	4	13.33	1.33	0.29	-0.04	0.33	0.61		
	0.7390-0.8133	116604	10.00	5	16.67	1.67	0.51	-0.08	0.59	1.2		
	0.8134-0.9078	116604	10.00	3	10.00	1.00	0.00	0.00	0.00	0		
	0.9079-1.0807	116575	9.99	2	6.67	0.67	-0.40	0.04	-0.44	-0.6		
	10.808-4.7295	116531	9.99	2	6.67	0.67	-0.40	0.04	-0.44	-0.6		
Li (ppb)	1.0000-1.0041	116661	10.00	6	20.00	2.00	0.69	-0.12	0.81	1.78	-0.18806	0.037
	1.0042-1.1144	116662	10.00	9	30.00	3.00	1.10	-0.25	1.35	3.39		
	1.1145-1.2670	116704	10.01	4	13.33	1.33	0.29	-0.04	0.32	0.6		
	1.2671-1.4984	116661	10.00	0	0.00	0.00	NaN	0.11	NaN	NaN		
	1.4985-1.9352	116631	10.00	2	6.67	0.67	-0.41	0.04	-0.44	-0.6		
	1.9353-2.6544	116633	10.00	2	6.67	0.67	-0.41	0.04	-0.44	-0.6		
	2.6545-3.5996	116624	10.00	3	10.00	1.00	0.00	0.00	0.00	0		
	3.5997-4.7935	116622	10.00	2	6.67	0.67	-0.41	0.04	-0.44	-0.6		
	4.7936-6.6524	116623	10.00	1	3.33	0.33	-1.10	0.07	-1.17	-1.15		
	6.6525-9.9999	116617	10.00	1	3.33	0.33	-1.10	0.07	-1.17	-1.15		
Mg (ppm)	0.36-1.12	116873	10.02	0	0.00	0.00	NaN	0.11	NaN	NaN	-0.00003	0.039
	1.13-2.50	117756	10.10	7	23.33	2.31	0.84	-0.16	1.00	2.31		
	2.51-3.04	118493	10.16	4	13.33	1.31	0.27	-0.04	0.31	0.57		
	3.05-3.64	117481	10.07	3	10.00	0.99	-0.01	0.00	-0.01	-0.01		
	3.65-4.41	116189	9.96	1	3.33	0.33	-1.09	0.07	-1.17	-1.15		
	4.42-5.26	116652	10.00	5	16.67	1.67	0.51	-0.08	0.59	1.2		
	5.27-6.18	116279	9.97	3	10.00	1.00	0.00	0.00	0.00	0.01		
	6.19-7.30	115792	9.93	5	16.67	1.68	0.52	-0.08	0.60	1.22		
	7.31-9.32	115912	9.94	1	3.33	0.34	-1.09	0.07	-1.16	-1.14		
	9.33-49.99	115011	9.86	1	3.33	0.34	-1.08	0.07	-1.15	-1.14		
Mn (ppb)	1.00-1.26	118658	10.17	4	13.33	1.31	0.27	-0.04	0.31	0.57	0.03390	0.033
	1.27-1.60	117500	10.07	2	6.67	0.66	-0.41	0.04	-0.45	-0.61		
	1.61-1.90	117854	10.10	7	23.33	2.31	0.84	-0.16	1.00	2.31		
	1.91-2.38	118036	10.12	4	13.33	1.32	0.28	-0.04	0.31	0.58		
	2.39-3.54	115883	9.93	2	6.67	0.67	-0.40	0.04	-0.43	-0.59		
	3.55-6.19	115970	9.94	5	16.67	1.68	0.52	-0.08	0.59	1.21		
	6.20-11.26	115651	9.91	1	3.33	0.34	-1.09	0.07	-1.16	-1.14		
	11.27-25.24	115647	9.91	1	3.33	0.34	-1.09	0.07	-1.16	-1.14		
	25.25-67.60	115630	9.91	3	10.00	1.01	0.01	0.00	0.01	0.02		
	67.61-199.99	115609	9.91	1	3.33	0.34	-1.09	0.07	-1.16	-1.14		

Factor	Likelihood ratio						Weight of evidence				Logistic	ANN
	Class[a]	No. of pixels	%Area	Mineral occ.	%occ.	LS	W^+	W^-	C	C/S(c)	Coefficient	Weight
Na (ppm)	0.2200-0.5790	116685	10.00	0	0.00	0.00	NaN	0.11	NaN	NaN	-0.00082	0.041
	0.5791-0.6504	116721	10.01	1	3.33	0.33	-1.10	0.07	-1.17	-1.15		
	0.6505-0.6959	116839	10.02	3	10.00	1.00	0.00	0.00	0.00	0		
	0.6960-0.7287	116664	10.00	3	10.00	1.00	0.00	0.00	0.00	0		
	0.7288-0.7844	116629	10.00	7	23.33	2.33	0.85	-0.16	1.01	2.33		
	0.7845-0.8366	116622	10.00	2	6.67	0.67	-0.41	0.04	-0.44	-0.6		
	0.8367-0.8943	116676	10.00	3	10.00	1.00	0.00	0.00	0.00	0		
	0.8944-0.9611	116614	10.00	5	16.67	1.67	0.51	-0.08	0.59	1.2		
	0.9612-1.1210	116524	9.99	3	10.00	1.00	0.00	0.00	0.00	0		
	1.1211-4.1488	116464	9.98	3	10.00	1.00	0.00	0.00	0.00	0		
Ni (ppb)	1.0001-5.3709	116644	10.00	1	3.33	0.33	-1.10	0.07	-1.17	-1.15	-0.71027	0.052
	5.3710-8.8292	116646	10.00	4	13.33	1.33	0.29	-0.04	0.33	0.61		
	8.8293-10.4420	116644	10.00	3	10.00	1.00	0.00	0.00	0.00	0		
	10.4421-11.6711	116651	10.00	5	16.67	1.67	0.51	-0.08	0.59	1.2		
	11.6712-12.7538	116655	10.00	1	3.33	0.33	-1.10	0.07	-1.17	-1.15		
	12.7539-13.9820	116648	10.00	2	6.67	0.67	-0.41	0.04	-0.44	-0.6		
	13.9821-14.9556	116644	10.00	1	3.33	0.33	-1.10	0.07	-1.17	-1.15		
	14.9557-15.9219	116646	10.00	1	3.33	0.33	-1.10	0.07	-1.17	-1.15		
	15.9220-16.7251	116633	10.00	7	23.33	2.33	0.85	-0.16	1.01	2.33		
	16.7252-19.9999	116627	10.00	5	16.67	1.67	0.51	-0.08	0.59	1.2		
Pb (ppb)	1.00-8.76	116772	10.01	1	3.33	0.33	-1.10	0.07	-1.17	-1.15	0.35117	0.041
	8.77-17.68	116678	10.00	5	16.67	1.67	0.51	-0.08	0.59	1.2		
	17.69-21.65	116889	10.02	0	0.00	0.00	NaN	0.11	NaN	NaN		
	21.66-24.56	117006	10.03	4	13.33	1.33	0.28	-0.04	0.32	0.6		
	24.57-27.30	116743	10.01	3	10.00	1.00	0.00	0.00	0.00	0		
	27.31-30.38	116786	10.01	2	6.67	0.67	-0.41	0.04	-0.44	-0.61		
	30.39-33.10	116634	10.00	1	3.33	0.33	-1.10	0.07	-1.17	-1.15		
	33.11-36.51	116709	10.01	4	13.33	1.33	0.29	-0.04	0.32	0.6		
	36.52-39.37	116345	9.97	5	16.67	1.67	0.51	-0.08	0.59	1.21		
	39.38-49.99	115876	9.93	5	16.67	1.68	0.52	-0.08	0.60	1.21		
Si (ppm)	10.801-16.979	116655	10.00	3	10.00	1.00	0.00	0.00	0.00	0	0.00182	0.039
	16.980-18.317	116728	10.01	0	0.00	0.00	NaN	0.11	NaN	NaN		
	18.318-19.271	116675	10.00	2	6.67	0.67	-0.41	-0.41	-0.44	-0.6		
	19.272-20.521	116693	10.00	5	16.67	1.67	0.51	-0.08	0.59	1.2		
	20.522-21.914	116619	10.00	5	16.67	1.67	0.51	-0.08	0.59	1.2		
	21.915-23.443	116686	10.00	2	6.67	0.67	-0.41	0.04	-0.44	-0.6		
	23.444-25.021	116607	10.00	1	3.33	0.33	-1.10	0.07	-1.17	-1.15		
	25.022-27.559	116627	10.00	4	13.33	1.33	0.29	-0.04	0.33	0.61		
	27.560-31.012	116583	9.99	2	6.67	0.67	-0.40	0.04	-0.44	-0.6		
	31.013-96.079	116565	9.99	6	20.00	2.00	0.69	-0.12	0.81	1.78		
Sr (ppb)	8.00-20.48	116702	10.00	2	6.67	0.67	-0.41	0.04	-0.44	-0.6	-0.01682	0.033
	20.49-42.65	116644	10.00	6	20.00	2.00	0.69	-0.12	0.81	1.78		
	42.66-57.42	116749	10.01	1	3.33	0.33	-1.10	0.07	-1.17	-1.15		
	57.43-66.48	116649	10.00	2	6.67	0.67	-0.41	0.04	-0.44	-0.6		
	66.49-71.81	116821	10.02	2	6.67	0.67	-0.41	0.04	-0.44	-0.61		
	71.82-76.94	116630	10.00	3	10.00	1.00	0.00	0.00	0.00	0		
	76.95-84.38	116686	10.00	7	23.33	2.33	0.85	-0.16	1.01	2.33		
	84.39-96.47	116540	9.99	3	10.00	1.00	0.00	0.00	0.00	0		
	96.48-134.78	116509	9.99	4	13.33	1.33	0.29	-0.04	0.33	0.61		
	134.79-499.92	116508	9.99	0	0.00	0.00	NaN	0.11	NaN	NaN		

Factor	Likelihood ratio						Weight of evidence				Logistic	ANN
	Class[a]	No. of pixels	%Area	Mineral occ.	%occ.	LS	W^+	W^-	C	C/S(c)	Coefficient	Weight
V (ppb)	10.000-10.001	116806	10.01	4	13.33	1.33	0.29	-0.04	0.32	0.6	0.30635	0.040
	10.002-10.320	116672	10.00	5	16.67	1.67	0.51	-0.08	0.59	1.2		
	10.321-10.744	116623	10.00	4	13.33	1.33	0.29	-0.04	0.33	0.61		
	10.745-11.616	116648	10.00	1	3.33	0.33	-1.10	0.07	-1.17	-1.15		
	11.617-12.435	116656	10.00	3	10.00	1.00	0.00	0.00	0.00	0		
	12.436-14.190	116633	10.00	4	13.33	1.33	0.29	-0.04	0.33	0.61		
	14.191-15.335	116625	10.00	1	3.33	0.33	-1.10	0.07	-1.17	-1.15		
	15.336-17.900	116593	10.00	5	16.67	1.67	0.51	-0.08	0.59	1.2		
	17.901-20.623	116598	10.00	3	10.00	1.00	0.00	0.00	0.00	0		
	20.624-99.985	116584	9.99	0	0.00	0.00	NaN	0.11	NaN	NaN		
W (ppb)	1.000-2.152	116858	10.02	1	3.33	0.33	-1.10	0.07	-1.17	-1.15	-0.08502	0.040
	2.153-2.458	116646	10.00	2	6.67	0.67	-0.41	0.04	-0.44	-0.6		
	2.459-2.683	116776	10.01	4	13.33	1.33	0.29	-0.04	0.32	0.6		
	2.684-2.988	116706	10.01	4	13.33	1.33	0.29	-0.04	0.32	0.6		
	2.989-3.363	116762	10.01	0	0.00	0.00	NaN	0.11	NaN	NaN		
	3.364-4.015	116577	9.99	5	16.67	1.67	0.51	-0.08	0.59	1.2		
	4.016-4.478	116788	10.01	4	13.33	1.33	0.29	-0.04	0.32	0.6		
	4.479-4.946	116606	10.00	6	20.00	2.00	0.69	-0.12	0.81	1.78		
	4.947-6.530	116366	9.98	4	13.33	1.34	0.29	-0.04	0.33	0.61		
	6.531-49.994	116353	9.98	0	0.00	0.00	NaN	0.11	NaN	NaN		
Zn (ppb)	1.00-3.28	117143	10.04	4	13.33	1.33	0.28	-0.04	0.32	0.6	0.06363	0.047
	3.29-4.34	117519	10.08	3	10.00	0.99	-0.01	0.00	-0.01	-0.01		
	4.35-5.21	117200	10.05	1	3.33	0.33	-1.10	0.07	-1.18	-1.16		
	5.22-6.13	116683	10.00	2	6.67	0.67	-0.41	0.04	-0.44	-0.6		
	6.14-7.22	116931	10.02	3	10.00	1.00	0.00	0.00	0.00	0		
	7.23-8.81	116420	9.98	3	10.00	1.00	0.00	0.00	0.00	0		
	8.82-11.02	116562	9.99	2	6.67	0.67	-0.40	0.04	-0.44	-0.6		
	11.03-13.62	116052	9.95	2	6.67	0.67	-0.40	0.04	-0.44	-0.6		
	13.63-21.96	115998	9.94	4	13.33	1.34	0.29	-0.04	0.33	0.62		
	21.97-49.99	115930	9.94	6	20.00	2.01	0.70	-0.12	0.82	1.79		
Magnetic anomaly (nT)	-145--101	128137	10.99	3	10.00	0.91	-0.09	0.01	-0.10	-0.17	-0.00592	0.040
	-100--92	121586	10.42	4	13.33	1.28	0.25	-0.03	0.28	0.52		
	-91--83	118890	10.19	6	20.00	1.96	0.67	-0.12	0.79	1.73		
	-82--76	131697	11.29	3	10.00	0.89	-0.12	0.01	-0.14	-0.22		
	-75--68	118478	10.16	3	10.00	0.98	-0.02	0.00	-0.02	-0.03		
	-67--59	115975	9.94	4	13.33	1.34	0.29	-0.04	0.33	0.62		
	-58--49	115502	9.90	0	0.00	0.00	NaN	0.10	NaN	NaN		
	-48--32	110107	9.44	4	13.33	1.41	0.35	-0.04	0.39	0.72		
	-31--9	105926	9.08	1	3.33	0.37	-1.00	0.06	-1.06	-1.05		
	-8-153	100140	8.59	2	6.67	0.78	-0.25	0.02	-0.27	-0.37		
Distance from fault (m)	0-120	119087	10.21	0	0.00	0.00	NaN	0.11	NaN	NaN	0.00004	0.040
	123-256	118526	10.16	4	13.33	1.31	0.27	-0.04	0.31	0.57		
	258-408	118732	10.18	3	10.00	0.98	-0.02	0.00	-0.02	-0.03		
	416-577	117138	10.04	6	20.00	1.99	0.69	-0.12	0.81	1.77		
	579-771	115748	9.92	5	16.67	1.68	0.52	-0.08	0.60	1.22		
	774-993	115764	9.92	2	6.67	0.67	-0.40	0.04	-0.43	-0.59		
	994-1268	115499	9.90	2	6.67	0.67	-0.40	0.04	-0.43	-0.59		
	1271-1632	115411	9.89	6	20.00	2.02	0.70	-0.12	0.82	1.8		
	1633-2292	115313	9.89	0	0.00	0.00	NaN	0.10	NaN	NaN		
	2294-6224	115220	9.88	2	6.67	0.67	-0.39	0.04	-0.43	-0.59		

Factor	Likelihood ratio						Weight of evidence				Logistic	ANN
	Class[a]	No. of pixels	%Area	Mineral occ.	%occ.	LS	W^+	W^-	C	C/S(c)	Coefficient	Weight
Lithology	Ogl	1064	0.09	0	0.00	0.00	NaN	0.00	NaN	NaN	-0.79271	0.038
	lgr	4841	0.42	0	0.00	0.00	NaN	0.00	NaN	NaN	-2.99730	
	Di	14	0.00	0	0.00	0.00	NaN	0.00	NaN	NaN	-3.16070	
	Hagr	245	0.02	0	0.00	0.00	NaN	0.00	NaN	NaN	-3.47459	
	Hb	2281	0.20	2	6.67	34.09	3.53	-0.07	0.73	4.91	10.07286	
	Oyb	1022	0.09	0	0.00	0.00	NaN	0.00	NaN	NaN	-0.51637	
	Qr	49757	4.27	2	6.67	1.56	0.45	-0.03	0.73	0.64	8.17128	
	Qd	533	0.05	0	0.00	0.00	NaN	0.00	NaN	NaN	-1.22621	
	Kad	136	0.01	0	0.00	0.00	NaN	0.00	NaN	NaN	-2.89905	
	Kbd	881	0.08	1	3.33	44.13	3.79	-0.03	1.02	3.76	12.63237	
	Kfl	3	0.00	0	0.00	0.00	NaN	0.00	NaN	NaN	-3.09662	
	Kgp	359	0.03	0	0.00	0.00	NaN	0.00	NaN	NaN	-1.04403	
	Kh	262	0.02	0	0.00	0.00	NaN	0.00	NaN	NaN	0.000	
	Kj	792	0.07	0	0.00	0.00	NaN	0.00	NaN	NaN	-1.76128	
	Kqp	520	0.04	0	0.00	0.00	NaN	0.00	NaN	NaN	-2.28572	
	Ksgr	9862	0.85	0	0.00	0.00	NaN	0.01	NaN	NaN	-2.77574	
	Jigr	19233	1.65	0	0.00	0.00	NaN	0.02	NaN	NaN	-3.95983	
	Jgr	3466	0.30	0	0.00	0.00	NaN	0.00	NaN	NaN	-1.67798	
	Jbs	584	0.05	0	0.00	0.00	NaN	0.00	NaN	NaN	-1.98813	
	Jbc	3969	0.34	0	0.00	0.00	NaN	0.00	NaN	NaN	-1.88599	
	TRn	20281	1.74	0	0.00	0.00	NaN	0.02	NaN	NaN	-0.62395	
	TRn1	20837	1.79	0	0.00	0.00	NaN	0.02	NaN	NaN	-1.69936	
	TRn2	12158	1.04	0	0.00	0.00	NaN	0.01	NaN	NaN	-1.51514	
	TRn3	6944	0.60	0	0.00	0.00	NaN	0.01	NaN	NaN	-1.19401	
	TRg	53754	4.61	0	0.00	0.00	NaN	0.05	NaN	NaN	-1.57190	
	Ps	18150	1.56	0	0.00	0.00	NaN	0.02	NaN	NaN	-2.17348	
	Ch	69942	6.00	0	0.00	0.00	NaN	0.06	NaN	NaN	-2.64278	
	Oj	78322	6.71	1	3.33	0.50	-0.70	0.04	1.02	-0.72	7.71043	
	Omg	215666	18.49	8	26.67	1.44	0.37	-0.11	0.41	1.14	9.53209	
	Odu	89243	7.65	4	13.33	1.74	0.56	-0.06	0.54	1.15	9.21845	
	Od	6794	0.58	0	0.00	0.00	NaN	0.01	NaN	NaN	-1.93977	
	CEw	129104	11.07	2	6.67	0.60	-0.51	0.05	0.73	-0.76	7.93944	
	CEp	112818	9.67	5	16.67	1.72	0.54	-0.08	0.49	1.28	8.46568	
	CEm	58514	5.02	2	6.67	1.33	0.28	-0.02	0.73	0.41	7.29037	
	CEj	17535	1.50	0	0.00	0.00	NaN	0.02	NaN	NaN	-3.67962	
	PCEt	103955	8.91	2	6.67	0.75	-0.29	0.02	0.73	-0.43	7.03664	
	Jugr	52597	4.51	1	3.33	0.74	-0.30	0.01	1.02	-0.31	6.39501	

[a]Using the quantile classification method

b_0: -18.75337 ; slope coefficients of the logistic regression

where W_i^+ and W_i^- of the binary pattern of each factors' class.

The magnitude of the contrast, C, is determined from the difference, W^+ and W^-. The Studentized C, calculated as the ratio of C to its standard deviation, C/s(C), serves as a guide to the statistical significance of the spatial association, and becomes useful in determining cutoff value to convert multiclass data into binary maps. The standard deviation of C is calculated as:

$$S(C) = \sqrt{S^2(W^+) + S^2(W^-)} \quad (6)$$

In this study the cutoff value was chosen based on the maximum Stucentized C. The binary maps were assigned weights (Table 1), and combined according to Equation (7). The mineral potential map using MPIW was shown in Figure 5.

$$MPI_W = \sum Woe, \quad (7)$$

where $Woe = W^+$ and W^- of the binary map for each factor.

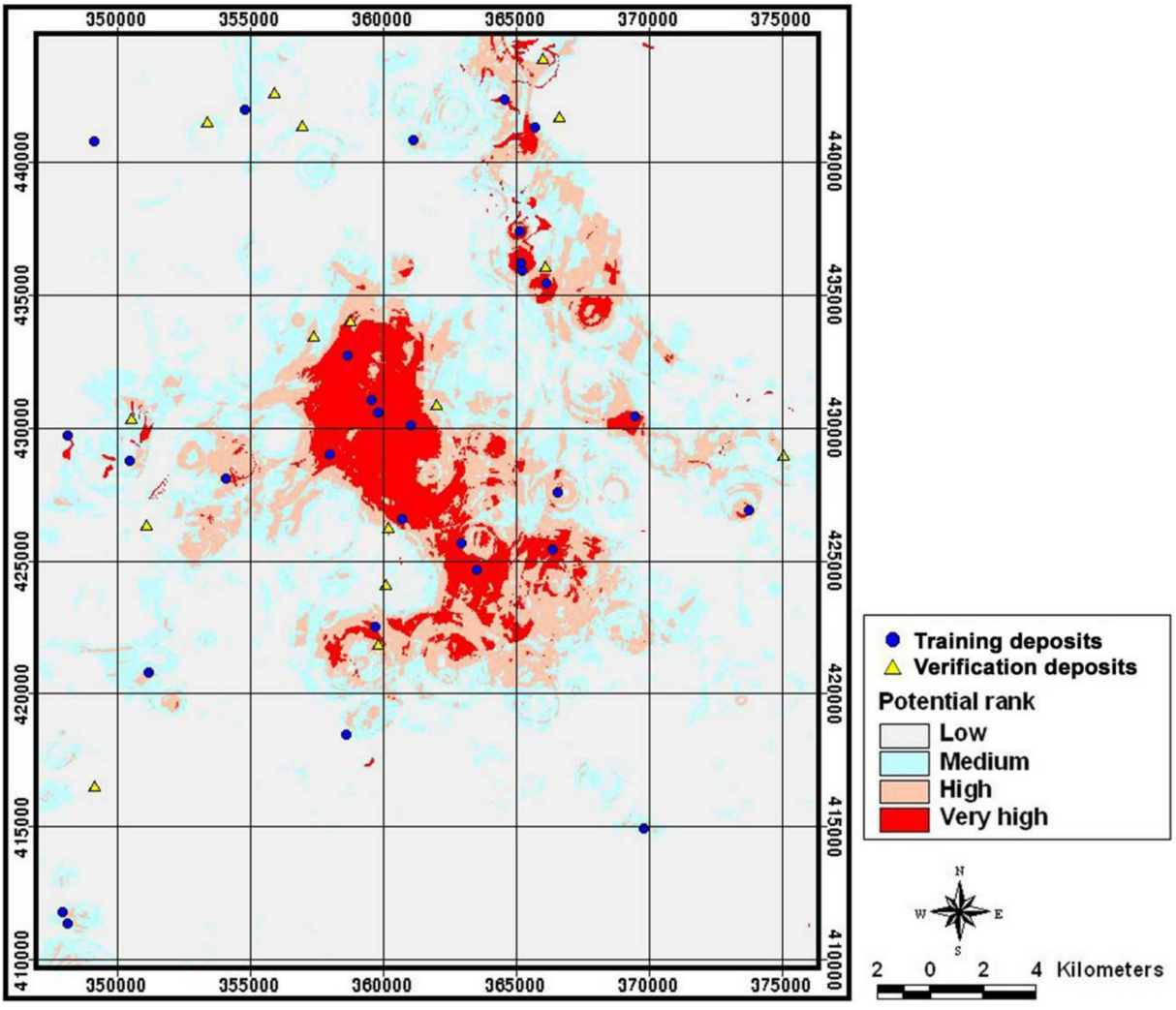

Figure 4. Au-Ag mineral potential map based on likelihood ratio model.

5.3. Logistic regression

Logistic regression is a multivariate analysis method. This is used to form a multivariate regression relation between independent variables (e.g., occurrence-related factors) and a dependent variable (e.g., a deposit occurrence). The advantage of logistic regression is that, through the addition of an appropriate link function to a usual linear regression model, the variables may be either continuous or discrete, or any combination of both types [26]. For this study, the dependent variable must be input as either 0 or 1 representing presence or absence of the deposit occurrence, so the method applies well to mineral potential analysis [1]. Logistic regression coefficients can be used to estimate odds ratios for each of independent variables in the model. The relationship between the deposit occurrence and its dependency on several variables can be expressed as:

$$p = \exp(z)/\big(1 + \exp(z)\big) \tag{8}$$

where p is the probability of the deposit occurrence and z is parameter. The probability varies from 0 to 1 on an S-shaped curve and z is the linear combination. It follows that logistic regression involves fitting an equation of the following form to the data:

$$z = b_0 + b_1 x_1 + b_2 x_2 + \cdots + b_n x_n \tag{9}$$

where b_0 is the y-axis intercept, $b_i (i = 0, 1, 2, \cdots, n)$ are the slope coefficients of the logistic regression model and $x_i (i = 0, 1, 2, \cdots, n)$ are the independent variables. The logistic regression coefficient values are listed in Table 1. The mineral potential map was made using MPI_{LO} (Equations (8) and (9)), shown in Figure 6.

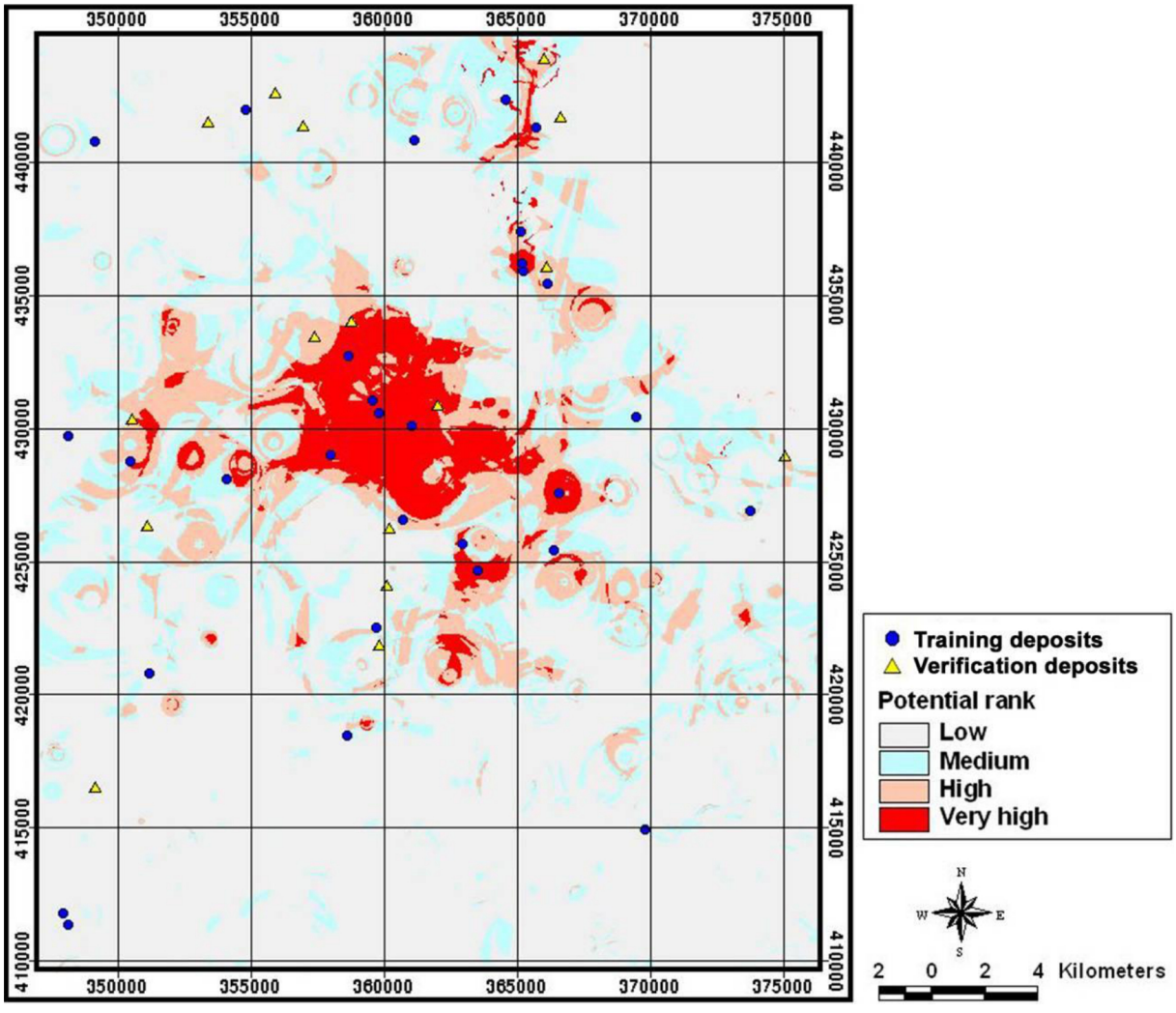

Figure 5. Au-Ag mineral potential map based on weight of evidence model.

5.4. Artificial neural network

The purpose of an artificial neural network is to build a model of the data-generating process so that the network can generalize and predict outputs from inputs [28]. Mineral potential was analyzed using an artificial neural network program that was partially modified and upgraded from the original version developed by Tsoukalas et al. [46] in the MATLAB package. For analysis of mineral potential, training sites were set to the locations of known deposit occurrence and non-occurrence. From each of the two classes, 30 grid cells per class were selected as training cells. The result of the likelihood ratio model was used to select training areas for supervised classification. Within the lower 10% of the mineral potential index values that were calculated by likelihood ratio model, 30 cells were selected randomly and the cells used as zero mineral potential areas. In addition, 30 cells of the known deposit used as areas susceptible to mineral potential. A three-layered feed forward network was implemented in MATLAB using the artificial neural network program. In this study, the 26 (input) × 52 (hidden) × 2 (output) structure was selected for the networks with input data normalized to the range 0.0 to 1.0. The learning rate parameter was set to 0.01 and the momentum parameter was set to 0.01. The selected deposit-prone training sites were assigned to values of (0.1, 0.9) and the non-deposit-prone training sites were assigned (0.9, 0.1). To lessen the error between the predicted output values and the actually calculated output values, the back propagation algorithm was used. The algorithm propagates the weights backwards and then controls the weights. The mineral potential index value was acquired by calculating the weights determined from back propaga-

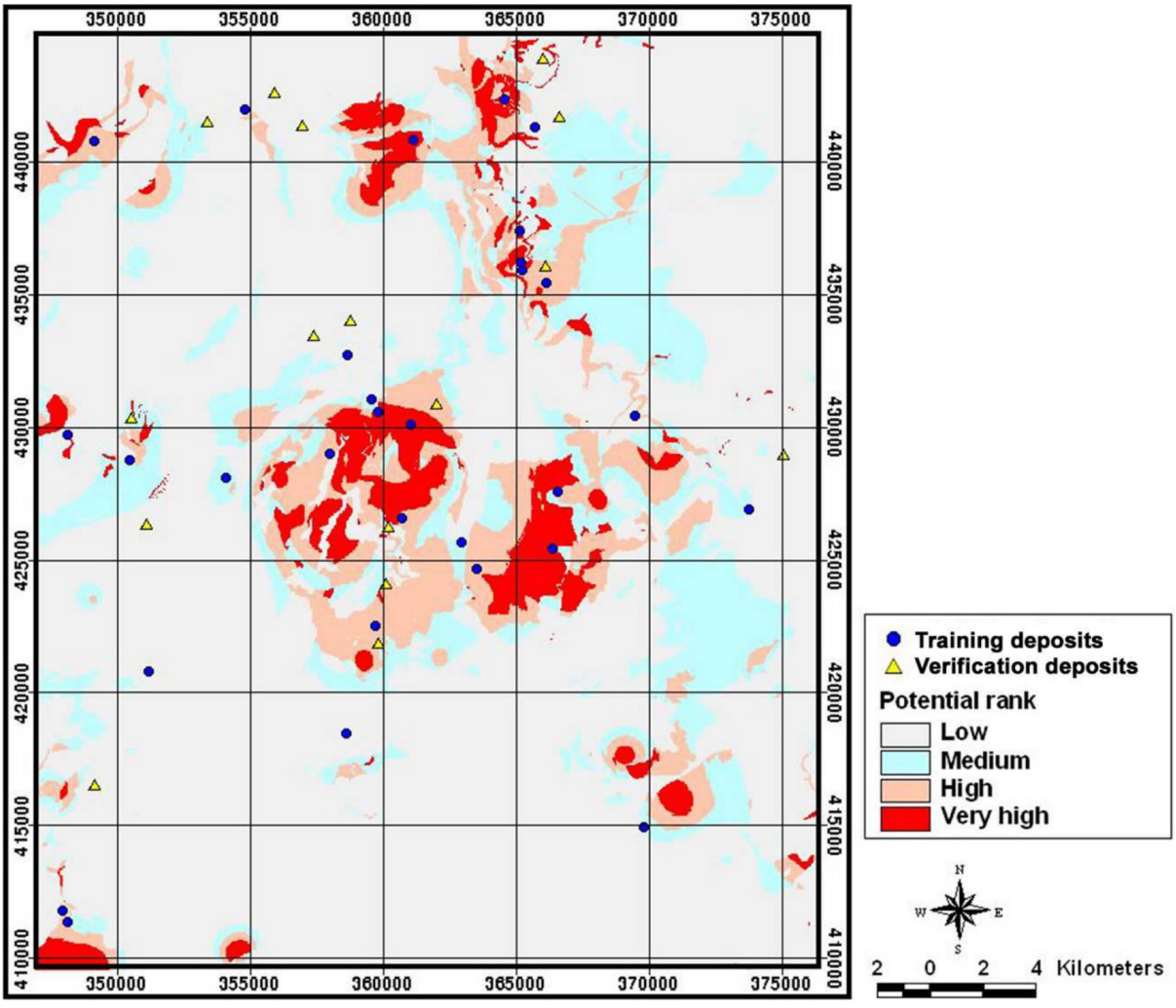

Figure 6. Au-Ag mineral potential map based on the logistic regression model.

tion and the spatial database. Then the mineral potential map was created. The weight and index values are shown in Table 1 and Figure 7.

6. Combining of mineral potential maps using likelihood ratio model

The mineral potential maps from likelihood ratio, weight of evidence, logistic regression and artificial neural network models were combined to make combined mineral potential map. For this, first, the mineral potential maps from each model were compared with mineral deposit using the likelihood ratio. The spatial relationship between mineral potential maps and mineral deposits is presented in Table 2. The ratio of each potential maps' class area for the total area was calculated and the likelihood ratios were ultimately obtained by dividing the mineral deposit-occurrence ratio by the ratio of each class.

The likelihood ratio value was set to the range of each mineral potential map values, which are reclassified into 10 classes to the equal area. The likelihood ratios for each class of mineral potential maps (Table 2) were summed to calculate $CMPI_L$ (Combined Mineral Potential Index), as shown in Equation (10):

$$CMPI_L = \sum MPI \tag{10}$$

where MPI = likelihood ratio for each class of four mineral potential maps (e.g., MPI_L, MPI_W, MPI_{LO}, and MPI_{ANN}). The combined mineral potential map that was made using Equation (10. If the $CMPI_L$ values are high, there exists a greater potential for a mineral deposit than where the

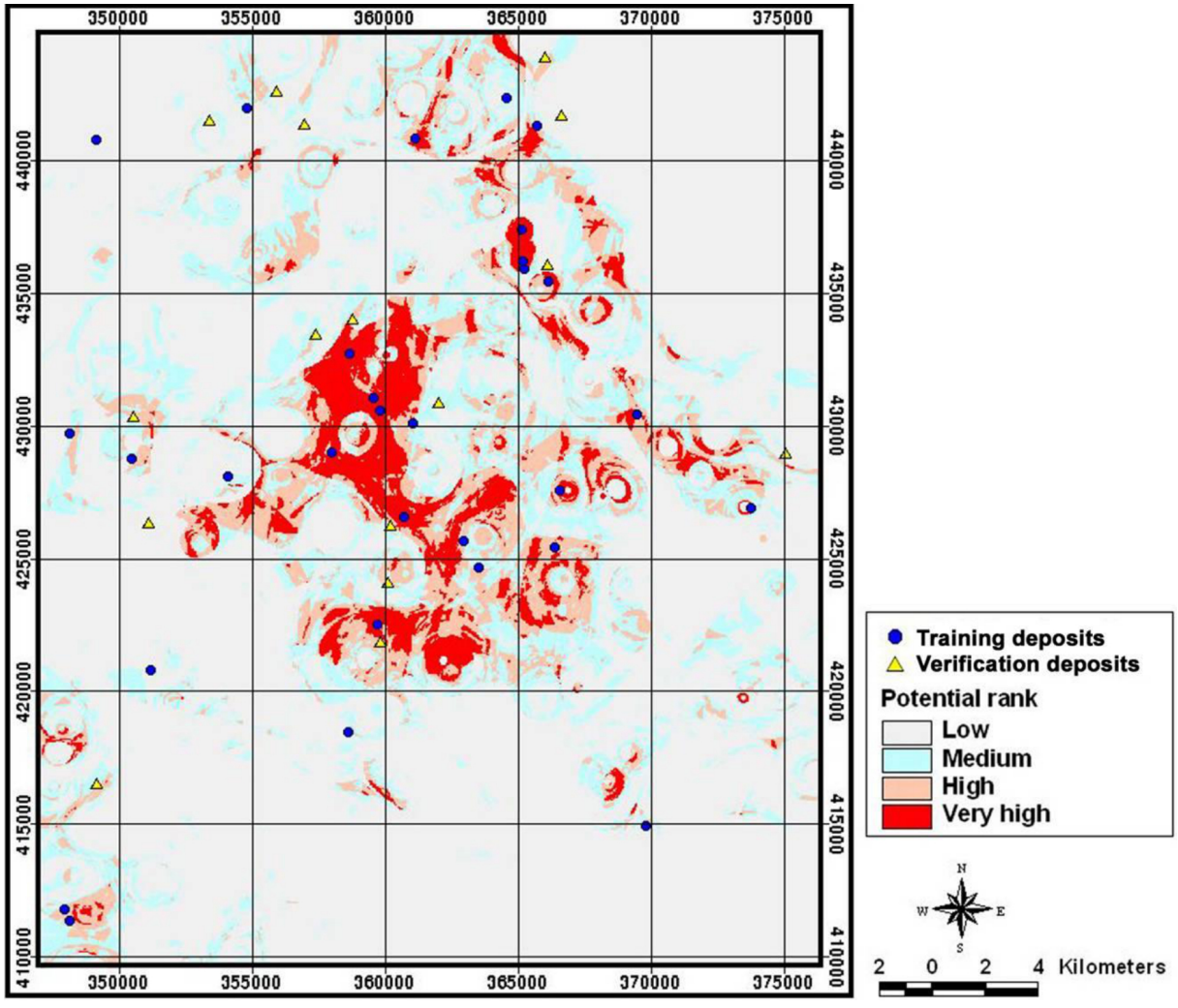

Figure 7. Au-Ag mineral potential map based on the artificial neural network model.

values are low. The index values for each mineral potential map were classified into four classes based on area for visual and easy interpretation; highest 5%, second 10%, third 15% and reminding 70% (Figures 4, 5, 6, 7 and 8).

7. Verification

The verification can ascertain the quality of mineral potential maps which created using the frequency ratio, weight of evidence, logistic regression and artificial neural network models. The verification method was performed by comparison of verification-mineral deposit data and mineral potential analysis results. For this, the success rate curves were drawn and the areas under the curve were determined in each case. The success rate shows how well the model and factors predict the mineral deposit occurrence; thus, the area under the curve qualitatively assesses the prediction accuracy. To obtain the relative ranking for each prediction pattern, the calculated values of all the cells in mineral potential map were sorted in the descending order. The ordered cell values were then divided into 100 classes with accumulated 1% intervals. As a result, the 90–100% class (10%) in which the mineral potential index had a high rank could explain 25%, 33%, 33% and 31% of all the mineral deposit occurrences using the likelihood ratio, weight of evidence, logistic regression and artificial neural networks models (Figure 9).

To compare the result quantitatively, the areas under the curve (AUC) were re-calculated as if the total area were one, which indicates perfect prediction accuracy [25]. The area beneath a curve can therefore be used to assess

Table 2. Likelihood ratio for each class of mineral potential maps analyzed from four different models.

Mineral potential map	Likelihood ratio					
	Class[a]	No. of pixels	%Area	Mineral occ.	%occ.	LS
MPI_L	10.24-18.40	117111	10.04	0	0.00	0.00
	18.41-21.07	117039	10.03	0	0.00	0.00
	21.08-23.03	116964	10.03	1	3.33	0.33
	23.04-24.58	116891	10.02	0	0.00	0.00
	24.59-25.99	116920	10.02	0	0.00	0.00
	26.00-27.48	116428	9.98	0	0.00	0.00
	27.49-29.04	116344	9.97	2	6.67	0.67
	29.05-30.81	116729	10.01	4	13.33	1.33
	30.82-33.36	116099	9.95	3	10.00	1.00
	33.37-62.28	115913	9.94	20	66.67	6.71
MPI_W	-2.92-2.63	152890	13.11	2	6.67	0.51
	-2.62-2.14	172099	14.75	3	10.00	0.68
	-2.13-1.79	105338	9.03	1	3.33	0.37
	-1.78-1.37	109198	9.36	0	0.00	0.00
	-1.36-1.13	104875	8.99	1	3.33	0.37
	-1.12-0.63	108054	9.26	1	3.33	0.36
	-0.62-0.22	104360	8.95	0	0.00	0.00
	-0.21-0.47	106455	9.13	5	16.67	1.83
	0.48-1.59	101870	8.73	4	13.33	1.53
	1.60-8.14	101299	8.68	13	43.33	4.99
MPI_{LO}	0	161883	13.88	0	0.00	0.00
	0.0000001-0.0000086	112363	9.63	0	0.00	0.00
	0.0000087-0.0000148	112165	9.62	0	0.00	0.00
	0.0000149-0.0000214	112221	9.62	0	0.00	0.00
	0.0000215-0.0000292	112001	9.60	3	10.00	1.04
	0.0000293-0.0000380	111232	9.54	1	3.33	0.35
	0.0000381-0.0000501	111880	9.59	4	13.33	1.39
	0.0000502-0.0000671	111408	9.55	7	23.33	2.44
	0.0000672-0.0000993	110854	9.50	4	13.33	1.40
	0.0000994-0.0042986	110431	9.47	11	36.67	3.87
MPI_{ANN}	0.0824-0.3497	116730	10.01	0	0.00	0.00
	0.3498-0.4999	116682	10.00	0	0.00	0.00
	0.5000-0.5929	116771	10.01	0	0.00	0.00
	0.5930-0.6648	116677	10.00	1	3.33	0.33
	0.6649-0.7199	116680	10.00	0	0.00	0.00
	0.7200-0.7681	116692	10.00	2	6.67	0.67
	0.7682-0.8135	116601	10.00	2	6.67	0.67
	0.8136-0.8577	116752	10.01	4	13.33	1.33
	0.8578-0.9014	116582	9.99	4	13.33	1.33
	0.9015-0.9748	116271	9.97	17	56.67	5.68

[a]Using the quantile classification method

the prediction accuracy qualitatively. The area under the curve is shown in Figure 9. The area ratios were 0.7224, 0.6585, 0.7223 and 0.7102 and we could say the prediction accuracies are 72.24%, 65.85%, 72.23% and 71.02%, respectively.

The combined mineral potential maps have verified using the same method. As a result, the 90–100% class (10%) and 80-100% class (20%) in whom the mineral potential index had a high rank could explain 50% and 56% of all the mineral deposit occurrences, respectively. The area ratio was 0.8397 and we could say the prediction accuracy is 83.97%.

8. Discussion and conclusion

A Geographic Information System (GIS) in concert with statistical software was used to compile, manipulate, analyze

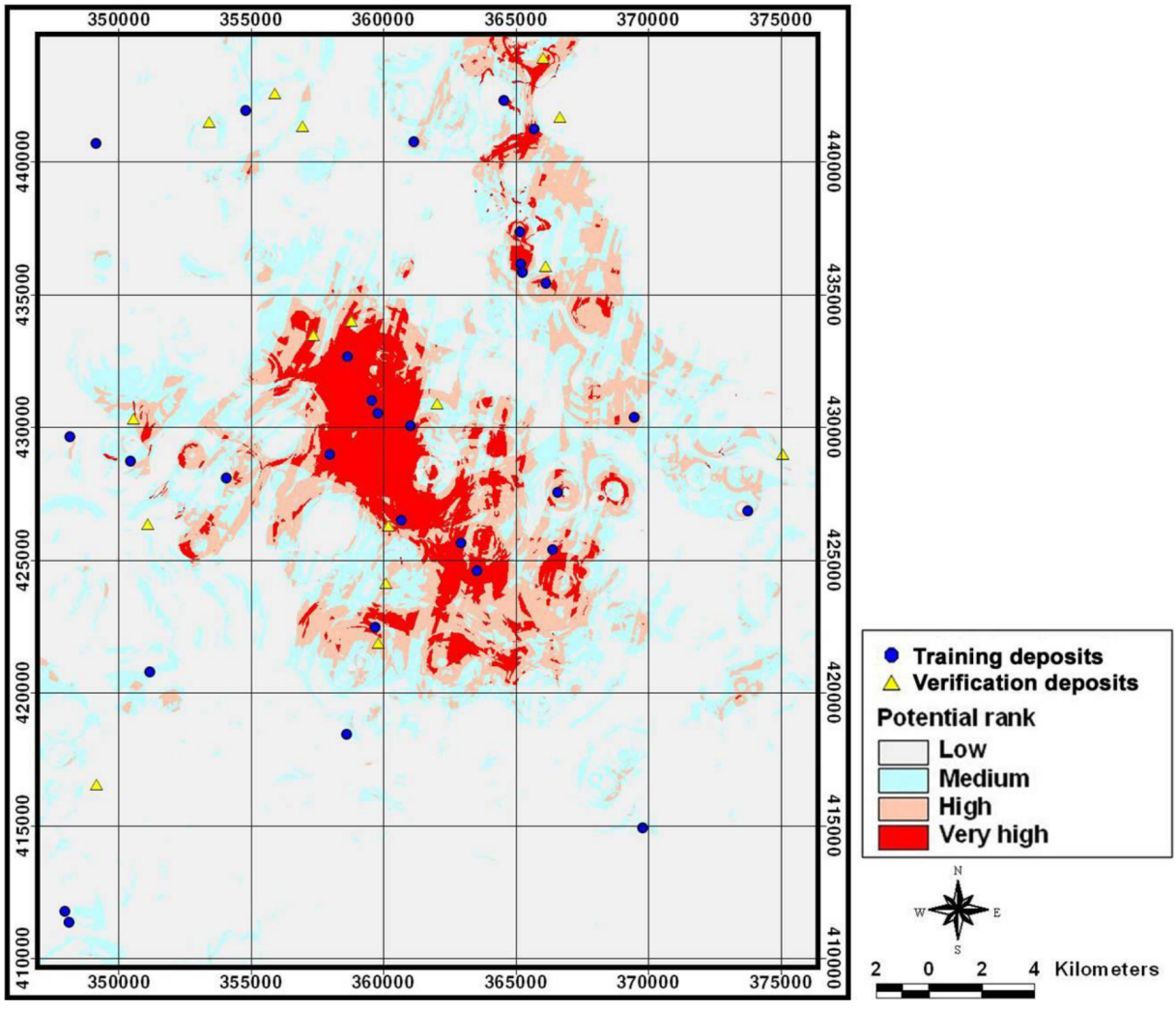

Figure 8. Combined Au-Ag mineral potential map based on likelihood ratio model.

and visualize a large geology, geochemical and geophysical dataset collected from the Taebaeksan mineralized area of Eastern Korea. The likelihood ratio, weight of evidence, logistic regression and artificial neural network models proved useful techniques for combining the geology, geochemical and geophysical maps produced in this study. Moreover, the combination of the models has applied to get the better accuracy than each model.

To compare the result quantitatively, we determined that the prediction accuracy. In the likelihood ratio model used, prediction accuracy was 72.24%. In the weight of evidence model, prediction accuracy was 65.85%, in the logistic regression model, prediction accuracy was 72.23% and in the artificial neural networks model, prediction accuracy was 71.02%. But the prediction accuracy for the combined mineral potential map was 83.97%. Overall, the combined mineral potential map gave higher accuracy than the each mineral potential map. We conclude that the combined models gave high prediction accuracy based on the mineral potential mapping in the study area.

The models are useful, not only for comparing the concentration of geochemical elements with the location of Au-Ag prospects, but also for providing a quantitative measure of the association between the concentration of geochemical elements and Au-Ag prospects. Furthermore, the maps generated by the models not only predict known areas of Au-Ag occurrence but also identify areas of potential mineralization where no known deposit occurs. A number of areas within the study area have been identified as having high Au-Ag potential. Many of these areas coincide with areas of known deposits. Others, however, are enigmatic and await follow-up exploration.

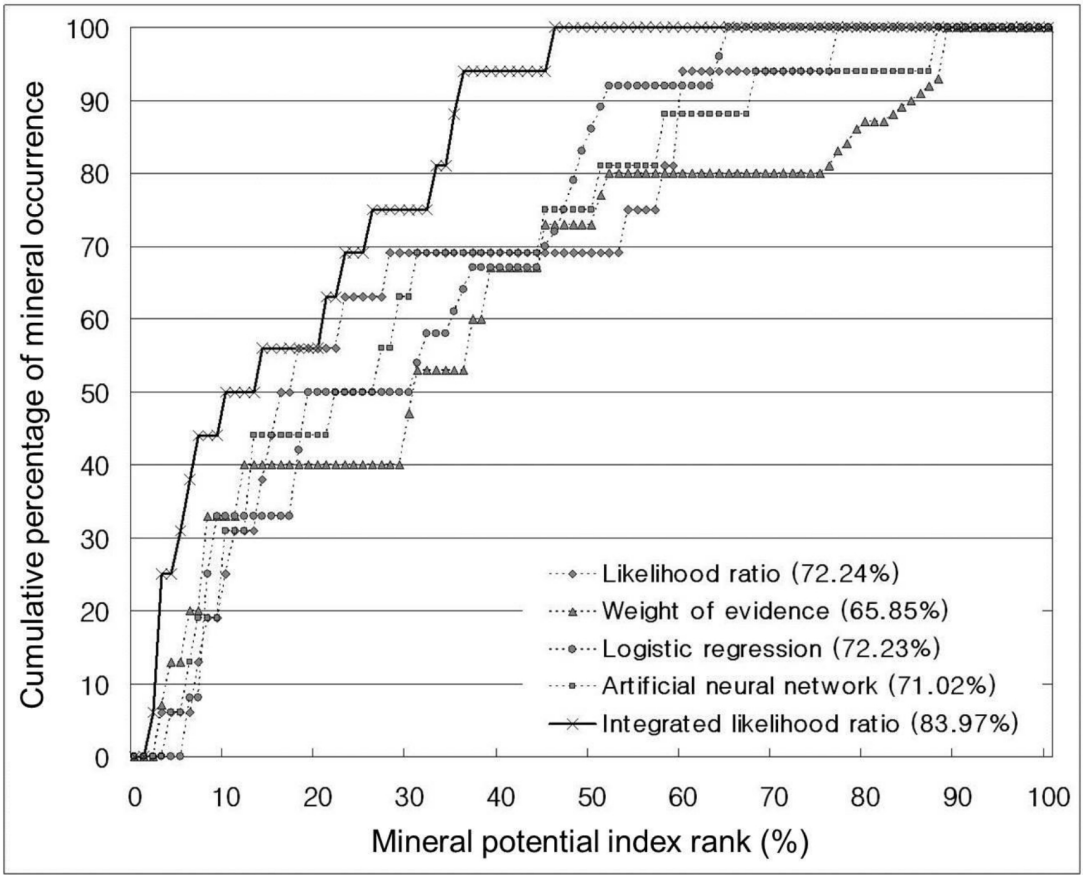

Figure 9. Illustration of cumulative frequency diagram showing mineral potential index rank (x-axis) occurring in cumulative percent of mineral deposit occurrence (y-axis).

Acknowledgments

This research was supported by the Basic Research Project (14-1121, 14-3311-1) of the Korea Institute of Geoscience and Mineral Resources (KIGAM) funded by the Ministry of Science, ICT and Future Planning.

References

[1] Atkinson P. M., Massari R., Generalised linear modelling of susceptibility to landsliding in the Central Apennines, Italy 1, *Computers & Geosciences*, 24, 1998, 373-385

[2] Bonham-Carter G., Geographic information systems for geoscientists: modelling with GIS, Pergamon, New York, 1994

[3] Bonham-Carter G. F., Agterberg F. P., Wright D. F., Weights of evidence modelling: a new approach to mapping mineral potential. In: Agterberg F. P. and Bonham-Carter G. F. (Ed.), Statistical Applications in the Earth Sciences, *Geological Survey of Canada Paper*, 1989, 171-183

[4] Brown W. M., Gedeon T. D., Groves D. I., Barnes R. G., Artificial neural networks: A new method for mineral prospectivity mapping, *Australian Journal of Earth Sciences*, 47, 2000, 757-770

[5] Carranza E. J. M, Weights of Evidence Modeling of Mineral Potential: A Case Study Using Small Number of Prospects, Abra, Philippines, *Natural Resources Research*, 13, 2004, 173-187

[6] Carranza E. J. M., Hale M., Logistic regression for geologically constrained mapping of gold potential, Baguio district, Philippines, *Exploration and Mining Geology*, 10, 2001,165-175

[7] Carranza E. J. M., Hale M., Faassen C., Selection of coherent deposit-type locations and their application in data-driven mineral prospectivity mapping, *Ore Geology Reviews*, 33, 2008, 536-558

[8] Cheng Q., Agterberg F. P., Fuzzy weights of evidence method and its application in mineral potential mapping, *Natural Resources Research*, 8, 1999, 27-35

[9] Cheong C. H., Lee H. Y., Ko I. S., Lee J. D., A study on stratigraphy and sedimentological environments of the lower Paleozoic sequences in South Korea (chiefly in Jeongseon area), *Journal of National Academy of Sciences, Republic of Korea*, 18, 1979, 123-159

[10] Cheong C. H., Stratigraphy and paleontology of the Samchang coalfield, Gangweondo, Korea, *The Journal of the Geological Society of Korea*, 26, 1969, 471-487

[11] Chi K. H., Lee J. S., Jin M. S., Chi S. J., Park S. H., Construction of GIS based geological database of South Korea Area. Korea Institute of Geoscience and Mineral Resources, Ministry of Science & Technology, KR-01(T)-08, 2001

[12] Chough S. K., Kwon S. T., Ree J. H., Choi D. K., Tectonic and sedimentary evolution of the Korean peninsula: A review and new view, *Earth Science Reviews*, 52, 2000, 175-235

[13] Chung C. F., Application of Recent Developments of Regression Analysis in Regional Mineral Resource Evaluation. In: Chung C. F., Fabbri A. G., Sinding-Larser R. (Ed.), *Quantitative Analysis of Mineral and Energy Resources*, Springer, Netherlands, 1987, 1-28

[14] D'Ercole C., Groves D. I., Knox-Robinson C. M., Using fuzzy logic in a geographic information system environment to enhance conceptually based prospectivity analysis of Mississippi Valley-type mineralisation, *Australian Journal of Earth Sciences*, 47, 2000, 913-927

[15] Devkota K., Regmi A., Pourghasemi H., Yoshida K., Pradhan B., Ryu I., Dhital M., Althuwaynee O., Landslide susceptibility mapping using certainty factor, index of entropy and logistic regression models and their comparison at a landslide prone area in Nepal Himalaya, *Natural Hazards*, 65, 2013, 135-165

[16] Kim J. C., Koh H. J., Lee S. R., Lee C. B., Choi S. J., Park K. H., *Explanatory note the Gangreung-Sokcho Sheet*. Korean Institute of Geoscience and Mineral Resources, Ministry of Commerce, industry and Energy, KR-M 25-08, 2001

[17] Kim J. H., Kee W. S., Tectonic significances of the Soon-Chang shear zone, the Hwasun coalfield, Korea, *Journal of the Geological Society of Korea*, 27, 1991, 642-655

[18] Kim J. H., Lee J. Y., Nam K. H., Pre-Jurassic thrust movement in Danyang area, Danyang coalfield, Korea, *Journal of the Geological Society of Korea*, 30, 1994, 35-40

[19] Kim J.H., Structure in the Taebaeksan zone, Structure and Metamorphism of the Ogcheon Belt: Field Trip Guidebook, *IGCP Project 321 Organizing Committee*, 1, 1994, 23-57

[20] Knox-Robinson C.M., Vectorial fuzzy logic: A novel technique for enhanced mineral prospectivity mapping, with reference to the orogenic gold mineralisation potential of the Kalgoorlie Terrane, Western Australia, *Australian Journal of Earth Sciences*, 47, 2000, 929-941

[21] Koh S.M., Kom S.Y., Lee D.J., Kim D.O., Lee H.Y., Kim Y.U., Yoo J.H., Kim Y.I., Ryoo C.R., Song M.S., *Construction of the data-base and assessment of domestic mineral resources III (Area of 1:250,000 Seoul and Gangreung Geological Sheets)*. Korean Institute of Geoscience and Mineral Resources, Ministry of Commerce, industry and Energy, KR-2002-C-14-2003-R, 2003

[22] Koo S.B., Cho J.D., Lee T.S., Park, Y.S., Lim M.T., Choi J.H., Sung N.H., Hwang H.S., Koh I.S., *Regional geophysical exploration*. Korean Institute of Geoscience and Mineral Resources, Ministry of Commerce, industry and Energy, KR-2000-R-11-2001-R, 2001

[23] Lee C.H., Park H.I., Epithermal gold-silver mineralization and depositional environment carbonate-hosted replacement type Baegjeon Deposits, Korea, *The Korean Society of Economic and Environmental Geology*, 1996, 29, 105-117

[24] Lee J.S., Seo H.J., Hwang I.H., *Regional geochemical mapping of the Kangneung Sheet (1:250,000)*, Korean Institute of Geoscience and Mineral Resources, Ministry of Commerce, industry and Energy, KR-98(C)-02, 1998

[25] Lee S., Dan N., Probabilistic landslide susceptibility mapping in the Lai Chau province of Vietnam: focus on the relationship between tectonic fractures and landslides, *Environmental Geology*, 48, 2005, 778-787

[26] Lee S., Ryu J.H., Kim I.S., Landslide susceptibility analysis and its verification using likelihood ratio, logistic regression, and artificial neural network models: Case study of Youngin, Korea, *Landslides*, 4, 2007, 327-338

[27] Mohammady M., Pourghasemi H.R., Pradhan B., Landslide susceptibility mapping at Golestan Province, Iran: a comparison between frequency ratio, Dempster-Shafer, and weights-of-evidence models, *Journal of Asian Earth Science*, 61, 2012, 221-236

[28] Oh H.J., Lee S., Application of artificial neural network for gold-silver deposits potential mapping: A case study of Korea, *Natural Resources Research*, 19, 2010, 103-124

[29] Oh H.J., Lee S., Regional probabilistic and statistical mineral potential mapping of gold-silver deposits using GIS in the Gangreung Area, Korea, *Resource Geology*, 58, 2008, 171-187

[30] Park M. E., James L. P., Sung K. Y., Sediment hosted disseminated and skarn gold mineralization in the Taebaegsan region, South Korea, *Geological Society*

of America, 2002 annual meeting, Denver (United States), 27-30 Oct, 2002

[31] Porwal A., Carranza E. J. M., Hale M., Artificial neural networks for mineral-potential mapping: a case study from Aravalli Province, Western India, *Natural resources research*, 12, 2003, 155-171

[32] Porwal A., Carranza E. J. M., Hale M., Bayesian network classifiers for mineral potential mapping, *Computers and Geosciences*, 32, 2006, 1-16

[33] Porwal A., Carranza E. J. M., Hale M., Knowledge-driven and data-driven fuzzy models for predictive mineral potential mapping, *Natural Resources Research*, 12, 2003, 1-25

[34] Pourghasemi H., Pradhan B., Gokceoglu C., Moezzi K. D., A comparative assessment of prediction capabilities of Dempster-Shafer and weights-ofevidence models in landslide susceptibility mapping using GIS, *Geomatics Nat. Hazards Risk*, 4, 2013, 93-118

[35] Pourghasemi H. R., Pradhan B., Gokceoglu C., Mohammadi M., Moradi H. R., Application of weights-of-evidence and certainty factor models and their comparison in landslide susceptibility mapping at Haraz watershed, Iran, *Arabian Journal of Geosciences*, 6, 2013, 2351-2365

[36] Pourghasemi H. R., Jirandeh A. G., Pradhan B., Xu C., Gokceoglu C., Landslide susceptibility mapping using support vector machine and GIS at the Golestan Province, Iran, *Journal of Earth System Science*, 122, 2013, 349-369

[37] Pradhan B., Flood susceptible mapping and risk area estimation using logistic regression, GIS and remote sensing, *Journal of Spatial Hydrology*, 9, 2009, 1-18

[38] Pradhan B., Mansor S., Pirasteh S., Buchroithner M. F., Landslide hazard and risk analyses at a landslide prone catchment area using statistical based geospatial model, *International Journal of Remote Sensing*, 32, 2011, 4075-4087

[39] Pradhan B., Oh H. J., Buchroithner M., Weights-of-evidence model applied to landslide susceptibility mapping in a tropical hilly area. Geomatics, *Natural Hazards and Risk*, 1, 2010, 199-223

[40] Pradhan B., Youssef A., Varathrajoo R., Approaches for delineating landslide hazard areas using different training sites in an advanced artificial neural network model, *Geo-spatial Information Science*, 13, 2010,93-102

[41] Rigol-Sanchez J. P., Chica-Olmo M., Abarca-Hernandez F., Artificial neural networks as a tool for mineral potential mapping with GIS, *International Journal of Remote Sensing*, 24, 2003, 1151-1156

[42] Skabar A., Modeling the spatial distribution of mineral deposits using neural networks, *Natural Resource Modeling*, 20, 2007, 435-450

[43] Sung K. Y., Park M. E., Yun S. T., Moon Y.H., Yoo I. K., Kim R. H., Shin J. K., Kim E. J., Geochemical Exploration for a Potential Estimation on the Carlin-type Gold Mineralization in Northern Mt. Taebaek Mining District, Korea, *The Korean Society of Economic and Environmental Geology*, 40, 2007, 537-549

[44] Tehrany M. S., Pradhan B., Jebur M. N., Flood susceptibility mapping using a novel ensemble weights-of-evidence and support vector machine models in GIS, *Journal of Hydrology*, 512, 2014, 332-343

[45] Tien Bui D., Pradhan B., Lofman O., Revhaug I., Dick O. B., Landslide susceptibility assessment in the Hoa Binh province of Vietnam: A comparison of the Levenberg-Marquardt and Bayesian regularized neural networks, *Geomorphology*, 171-172, 2012, 12-19

[46] Tsoukalas L. H., Uhrig R. E., and Zadeh L. A., *Fuzzy and Neural Approaches in Engineering, MATLAB Supplement*. Wiley, 1997